First publ. in: Journal of Biological Chemistry 276 (2001), 32, pp. 30435-30441

Oxygen Access to the Active Site of Cholesterol Oxidase through a Narrow Channel Is Gated by an Arg-Glu Pair*

René Coulombe‡, Kimberley Q. Yue‡, Sandro Ghisla§, and Alice Vrielink‡¶‖

From the ‡Department of Biochemistry and Montréal Joint Center for Structural Biology, McIntyre Medical Sciences Building, McGill University, Montréal, Québec H3G 1Y6, Canada, Fachbereich Biologe, University of Konstanz, D-78457 Konstanz, Germany, and ¶Departments of Biology and Chemistry, Sinsheimer Laboratory, University of California Santa Cruz, Santa Cruz, California 95064

Cholesterol oxidase is a monomeric flavoenzyme that catalyzes the oxidation and isomerization of cholesterol to cholest-4-en-3-one. Two forms of the enzyme are known, one containing the cofactor non-covalently bound to the protein and one in which the cofactor is covalently linked to a histidine residue. The x-ray structure of the enzyme from *Brevibacterium sterolicum* containing covalently bound FAD has been determined and refined to 1.7-Å resolution. The active site consists of a cavity sealed off from the exterior of the protein. A model for the steroid substrate, cholesterol, can be positioned in the pocket revealing the structural factors that result in different substrate binding affinities between the two known forms of the enzyme. The structure suggests that Glu^{475}, located at the active site cavity, may act as the base for both the oxidation and the isomerization steps of the catalytic reaction. A water-filled channel extending toward the flavin moiety, inside the substrate-binding cavity, may act as the entry point for molecular oxygen for the oxidative half-reaction. An arginine and a glutamate residue at the active site, found in two conformations are proposed to control oxygen access to the cavity from the channel. These concerted side chain movements provide an explanation for the biphasic mode of reaction with dioxygen and the ping-pong kinetic mechanism exhibited by the enzyme.

Cholesterol oxidase is a flavoprotein that catalyzes the oxidation and isomerization of steroids containing a 3β-hydroxyl group and a double bond at C-5 of the steroid ring system (see Scheme 1). The enzyme has been used in the determination of serum cholesterol and in the clinical diagnosis of arteriosclerosis and other lipid disorders. In addition, it has been shown to be a potent larvicide (1–3) and is currently being developed in the agricultural industry as a pest control (4). Furthermore, cholesterol oxidase is an example of a soluble enzyme that interacts with a lipid bilayer to bind an insoluble substrate. Structural and biochemical studies on the enzyme containing the flavin adenine dinucleotide (FAD)[1] cofactor non-covalently bound to the protein have revealed the region of the enzyme involved in interaction with the lipid bilayer and have led to a possible mechanism for membrane interaction (5–7).

In *Brevibacterium sterolicum*, cholesterol oxidase has been found to exist in two forms, one in which the FAD cofactor is non-covalently bound to the enzyme (BCO1) and one in which the cofactor is covalently linked (BCO2). Although these enzymes share the same catalytic activity they show no sequence homology. Comparisons of these two forms of cholesterol oxidase reveal large differences in redox potential and kinetic properties suggesting different mechanisms (8). These studies support the hypothesis that there are significant structural differences between the two enzyme forms, correlated with changes in biochemical properties.

Here we report the structure of BCO2 refined to 1.7-Å resolution. The structure reveals features of the enzyme that support previously proposed models of both substrate binding and catalysis. Furthermore, specific active site residues can now be implicated in the mechanisms for oxidation, isomerization, and for the oxidative half-reaction of the enzyme.

EXPERIMENTAL PROCEDURES

Data Collection and Processing—Pure recombinant BCO2 was obtained from Roche Molecular Diagnostics. Crystals were grown by vapor diffusion as described previously (9). The crystals belong to space group P21 with unit cell dimension a = 77.44 Å, b = 124.47 Å, c = 80.84 Å, and β = 109.2° and contain 2 molecules in the asymmetric unit. Prior to data collection the crystals were briefly soaked in a cryoprotectant solution containing 20% ethanediol. Data for the low resolution native crystal and the mercurial derivatives were collected on a MAR image plate detector with a double focussing mirror system (Supper, Ltd.) mounted on a Rigaku RU-200 rotating anode x-ray generator. The high-resolution native data were collected at 0.979 Å on beamline X8-C (NSLS, Brookhaven National Laboratory, New York). The x-ray images were processed using the HKL suite of software (10, 11). Table I gives the data collection and processing statistics.

Phase Determination and Refinement—The structure was solved by the method of single isomorphous replacement using a mercurial derivative ($HgCl_2$). Two different soak concentrations of the heavy atom solution were used giving slightly different phase information (see Tables I and II). Heavy atom refinement was carried out using the program MLPHARE. The initial phases from heavy atom refinement of two mercurial sites were significantly improved by solvent flipping using SOLOMON (12). A partial model was built for each protomer in the asymmetric unit and used to determine the non-crystallographic symmetry matrices. The program DM was used to further improve the phases by 2-fold averaging, solvent flattening, and histogram matching. The improved quality of the electron density map enabled a more complete model to be built. The model phases were gradually combined with the MIR phases using SIGMAA and the resulting maps used to

* This work was supported by Canadian Institutes of Health Research Grant MT13341 (to A. V.), National Institutes of Health Grant GM60535 (to A. V.), and a chercheur-boursier salary support award from the Fonds de la recherche en santé du Québec (to A. V.). The costs of publication of this article were defrayed in part by the payment of page charges. This article must therefore be hereby marked "*advertisement*" in accordance with 18 U.S.C. Section 1734 solely to indicate this fact.

‖ To whom correspondence should be addressed: Dept. of Biology, Sinsheimer Lab., University of California Santa Cruz, 1156 High St., Santa Cruz, CA 95064. Tel.: 831-459-3929; Fax: 831-459-3139; E-mail: vrielink@biology.ucsc.edu.

[1] The abbreviations used are: FAD, flavin adenine dinucleotide; VAO, vanillyl alcohol oxidase; r.m.s., root mean square.

SCHEME 1.

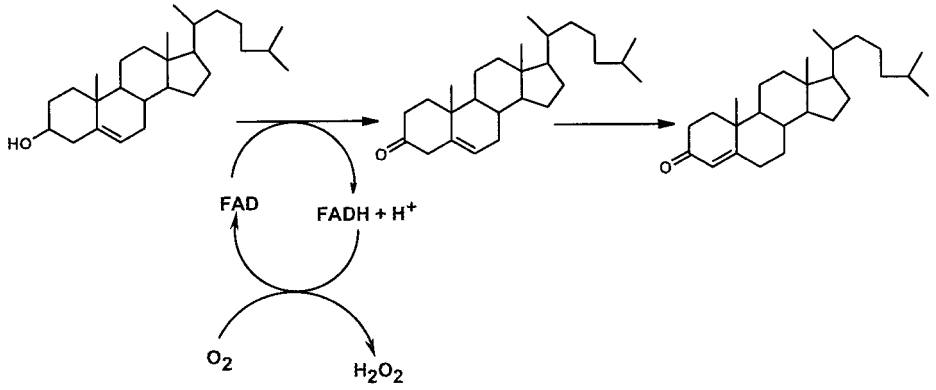

TABLE I
Crystallographic statistics for cholesterol oxidase

Data collection

Dataset	Soak conditions	Resolution[a]	Total reflections	Unique reflections	I/σ	Completeness	R_{merge}
		Å				%	
Native 1		2.4	159,332	53,139	15.1	92.4 (72.4)	0.044
Native 2		1.7	550,182	150,202	16.4	94.8 (68.4)	0.065
$HgCl_2$	0.1 mM (30 min)	2.8	70,989	33,778	15.5	92.3 (67.6)	0.052
$HgCl_2$	0.05 mM (30 min)	2.8	52,177	33,987	16.4	93.3 (75.4)	0.044

[a] Data in the highest resolution bin.

TABLE II
Refinement statistics

Model refinement statistics	
Resolution range (Å)	37–1.7
Total reflections used in refinement	150,168
R factor[a]	0.182
Free R factor[b]	0.201
r.m.s.d. bond lengths (Å)	0.006
r.m.s.d. bond angles (°)	1.3
Number of non-hydrogen atoms	9582
Average B factors (Å^2)	19.8

[a] R factor = $\Sigma\Sigma_h||F_{obs}(h)| - k|F_c(h)||/\Sigma_h|F_{obs}(h)|$.
[b] Free R factor was calculated using a 10% randomly selected subset of the total number of reflections.

complete building of the model. Model building was performed with O (13) and refinement carried out with CNS (14) using the high-resolution data (Native 2). Each cycle of refinement was followed by a manual rebuild using the program O. SIGMAA weighted maps calculated with coefficients $3F_o - 2F_c$ and $F_o - F_c$ were used for the model rebuilds. In the final stages of refinement $2F_o - F_c$ maps were used. Water molecules were built where difference electron density above 3σ was observed and where hydrogen bond contacts were made to other polar atoms. As the refinement neared completion, difference electron density maps indicated the presence of 12 molecules of ethanediol, 3 Mn^{2+} ions, and 1 cacodylate molecule. In the final stages of refinement the NCS constraints were removed and multiple conformations for the side chains of 46 residues as well as one ethanediol molecule located in the active site were included. A surface exposed loop in each protomer was not included in the final model since the density was not sufficiently well defined. Superposition of identical α-carbon positions for the two molecules results in an r.m.s. difference of 0.27 Å indicating that the two subunits are structurally identical. The Ramachandran plot indicates that all residues lie in allowed regions of φ/ψ space (15). The final refinement statistics are given in Table II. The atomic coordinates and structure factors have been deposited in the Brookhaven Protein Data Bank (16) (accession codes 1I19).

RESULTS AND DISCUSSION

Overall Structure—Cholesterol oxidase (BCO2) from *B. sterolicum* containing FAD covalently attached to the protein is a monomeric enzyme of 613 amino acid residues. The full-length enzyme contains a hydrophobic presequence of 52 residues, the function of which is currently not known. The protein is cleaved after residue 52 to give the 62-kDa mature form of the enzyme. The structure for the mature enzyme has been determined by the method of single isomorphous replacement and refined to 1.7-Å resolution.

The structure is composed of 12 α-helices and 17 β-strands and can be subdivided into two functionally distinct domains: an FAD-binding domain and a substrate-binding domain (Fig. 1). Although BCO2 carries out an identical catalytic reaction to that of BCO1, the structural folds for the two enzymes are vastly different. In particular, the nucleotide binding fold commonly seen in the FAD-binding domain is not present in BCO2; rather it adopts a fold seen in the structures of vanillyl alcohol oxidase (VAO) (17), murB (18), the molybdenum-containing enzyme carbon monoxide dehydrogenase (19), and *p*-cresol methylhydroxylase (20). This fold has recently been described as a new family of structurally related oxidoreductases (21). The r.m.s. deviation for 140 α-carbon atoms within the FAD-binding domain between VAO and BCO2 is 1.7 Å. Although BCO2 was not originally included in this family of enzymes due to the lack of sequence homology, the observed structure homology indicates that it is also a member of this new oxidoreductase family.

The substrate-binding domain (residues 275–565) is comprised of an 8-stranded mixed β-pleated sheet and 6 α-helices. This domain is positioned over the isoalloxazine ring system of the FAD cofactor and forms the roof of the active site cavity. The motif for this domain is also observed in the structures of VAO and *p*-cresol methylhydroxylase although there is no significant sequence homology between these enzymes and BCO2. Superposition of 94 α-carbon atoms within the substrate-binding domains of BCO2 and VAO results in an r.m.s. deviation of 2.1 Å.

FAD Binding—The FAD is deeply buried in the protein structure and is involved in extensive contacts mainly with the FAD-binding domain. The pyrophosphate group is involved in hydrogen bond contacts with main chain atoms of the loop between Gly^{118} and Gly^{122}. A similar type of interaction has

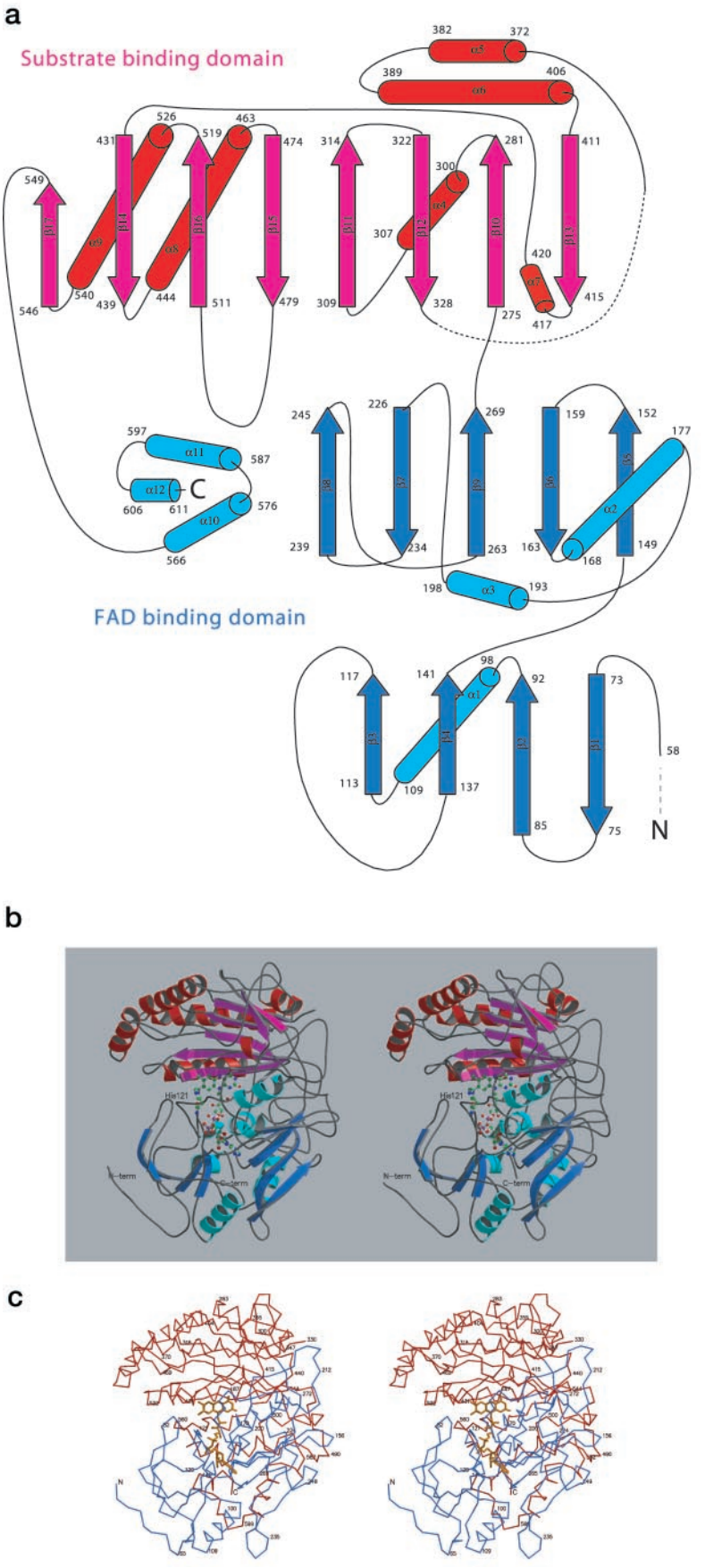

FIG. 1. *a,* topology diagram for cholesterol oxidase. The strands and helices are numbered in the order that they appear in the primary sequence. *b*, stereo figure showing a ribbon representation of BCO2 (produced with the program Molscript (31)). The FAD cofactor and His^{121} are shown in a ball-and-stick representation with *white colored* bonds. *c,* stereo figure showing the α carbon trace of BCO2 with various residues along the chain tracing labeled. The FAD-binding domain is colored *blue* and the substrate-binding domain is *red*. The FAD cofactor is shown as a *yellow* stick representation.

also been observed in the structure of VAO and this loop region has been defined as the PP loop (17).

The cofactor is linked to the protein through a covalent bond between ND1 of the imidazole side chain of His^{121} (a residue in the PP loop) and the 8-methyl group of the isoalloxazine ring (Fig. 2). The histidine side chain approaches the isoalloxazine

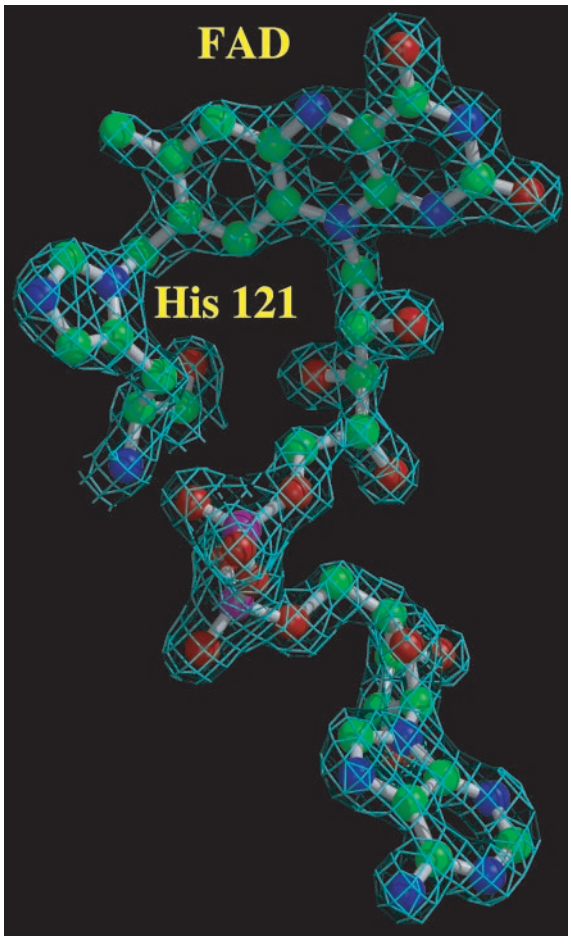

FIG. 2. **Electron density for the FAD cofactor and the covalently bound Histidine residue (121) of cholesterol oxidase.** The electron density is from a $2F_o - F_c$ map contoured at 1.5σ.

ring from the *si* face of the flavin unlike VAO where the covalent histidine originates in the substrate-binding domain and approaches the flavin moiety from the *re* face. Therefore, in BCO2, the PP loop appears to play a critical role in positioning the cofactor correctly within the structure of the enzyme through two factors: the covalent linkage to the isoalloxazine ring and the hydrogen bond interactions with the pyrophosphate moiety.

A number of flavoenzymes have been found to contain a covalent linkage between the cofactor and the protein (reviewed by Mewies *et al* (22)). The structures of covalently modified flavoenzymes that have been determined include VAO (17), where the covalent linkage is through ND2 of a histidine residue and *p*-cresol methylhydroxylase (20) where the linkage is through a tyrosine residue. BCO2 represents the first structure within this family where the protein-flavin linkage is through the ND1 atom of a histidine residue and from the *re* face of the isoalloxazine ring system.

Active Site—The active site of BCO2 consists of a cavity (with a volume of 450 Å^3) bounded on one side by the β-pleated sheet in the substrate-binding domain and, on the opposite side, by the isoalloxazine ring of the cofactor. Two loops in the substrate-binding domain (between β12 and α5 and between α7 and β14) exhibit higher than average temperature factors suggesting a possible entrance for cholesterol to the active site (Fig. 3*a*). The residues lining the cavity near the pyrimidine moiety of the cofactor are highly hydrophilic and include Arg^{477}, Glu^{475}, Glu^{551}, Glu^{432}, Glu^{311}, Asn^{516}, and Lys^{554} (Fig. 3*b*). The charged nature of this region of the active site is in

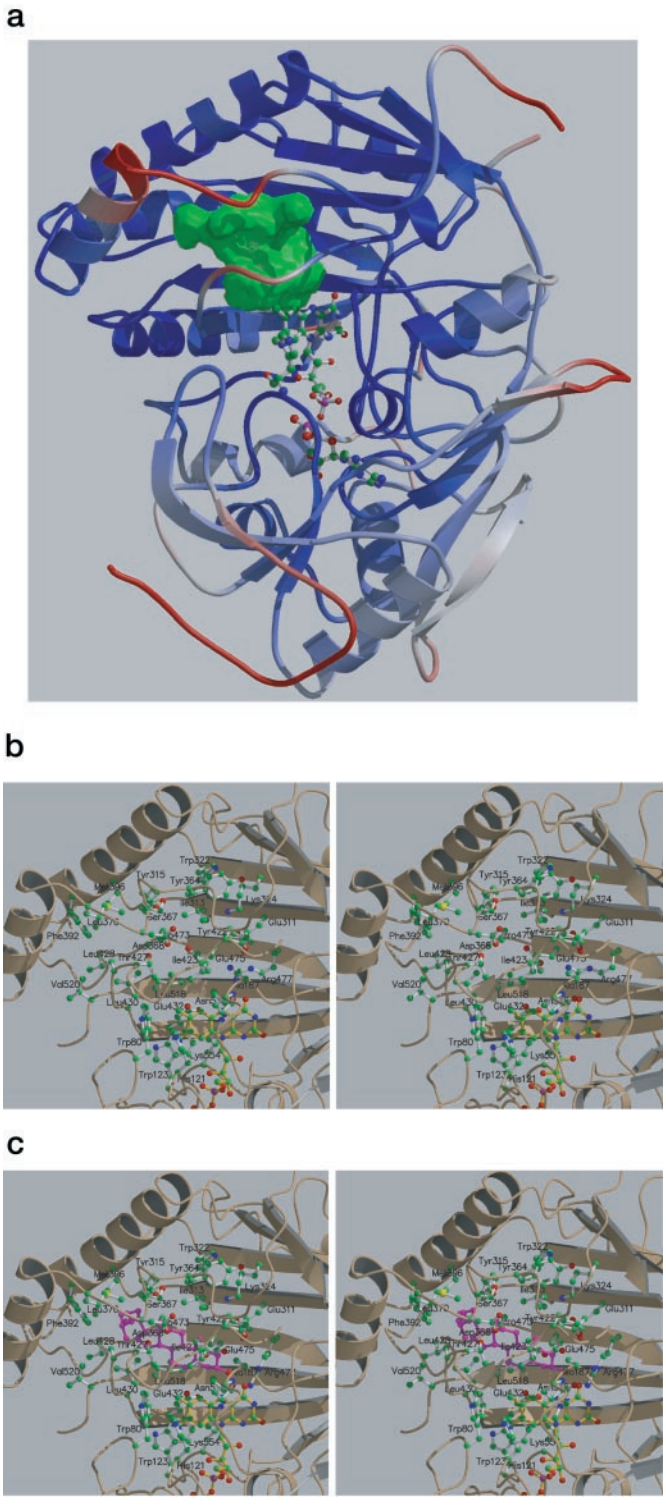

FIG. 3. *a,* secondary structure diagram of cholesterol oxidase showing a surface representation of the internal cavity that accommodates a cholesterol substrate molecule. The secondary structure elements of the protein are colored according to average main chain temperature factors. *Dark red* corresponds to temperature factors over 32 Å^2 and *dark blue* to temperature factors under 15 Å^2. *b,* stereo view showing substrate-binding site in the gate open conformation. *c,* stereo view showing the model for cholesterol bound to the substrate-binding site in the gate closed conformation. The amino acid side chain that line the cavity are shown with *white bonds*, the FAD cofactor is shown with *yellow bonds,* and the cholesterol substrate is colored *magenta*.

sharp contrast to that seen in the structure of BCO1 and it is precisely these differences that are likely to play an important role in the reactivity of the flavin cofactor. The region near to

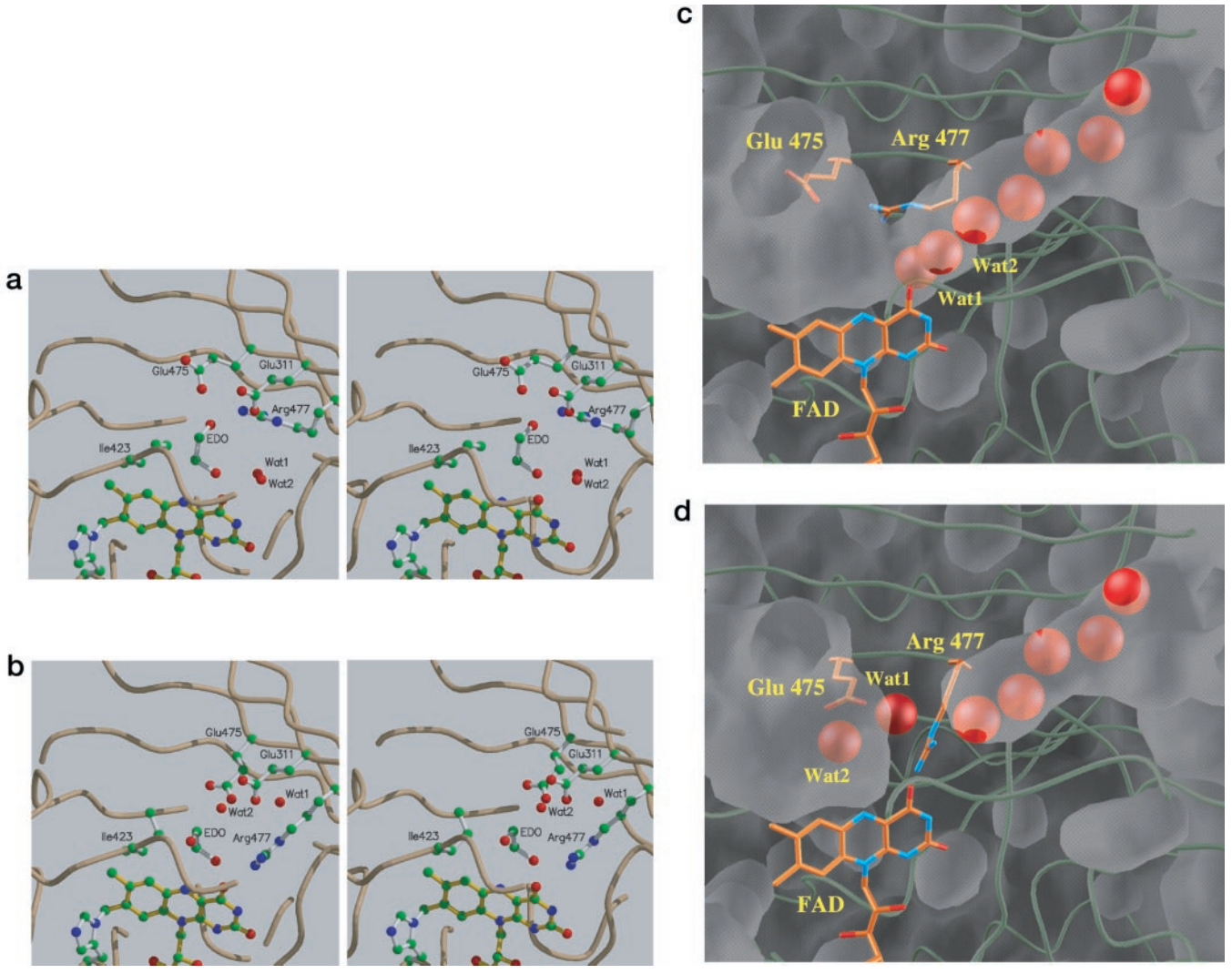

FIG. 4. The figure contains a stereo view showing (*a*) the gate open conformation and (*b*) the gate closed conformation of the active site. The bound ethanediol molecule is labeled as EDO and water molecules are shown as *red spheres*. *c*, surface representation showing the proposed oxygen channel with the gate open, and *d,* the gate closed conformation at the active site. The molecular surface is constructed using the program GRASP (32). The protein main chain is shown as a *green coil*. The FAD cofactor is shown in *yellow*, the side chains for Arg^{477} and Glu^{475} are included and the water molecules are shown as *red* CPK spheres.

the dimethylbenzene ring of the cofactor consists mainly of hydrophobic residues. An extension away from the main cavity and lined by hydrophobic residues is also observed.

Three side chains in the active site: Arg^{477}, Glu^{475}, and Ile^{423} adopt two distinct conformations (Fig. 4). Their movements appear to be coordinated with each other and with alternate positions of two water molecules and one ethanediol in the active site. In one conformation, the guanidinium group of Arg^{477} is within hydrogen bonding distance from O-4 of the isoalloxazine ring and the hydroxyl O-2 of ethanediol (Fig. 4*b*). The second hydroxyl group of ethanediol, O-1, makes contact with N-5 of FAD, and the side chain of Ile^{423} is directed away from the active site cavity. In the second conformation, the side chain of Arg^{477} has swung away from the cofactor and contacts the carboxylate group of Glu^{475} which has also moved away to accommodate the arginine side chain (Fig. 4*a*). Two water molecules occupy the original position of Arg^{477} near O-4 of the cofactor. Furthermore, the ethanediol molecule has adopted an alternate conformation such that O-2 interacts with one of the new water molecule positions and O-1 interacts with the newly positioned Arg^{477}. This alternate conformation of ethanediol results in a repositioning of side chain of Ile^{423}, toward the active site cavity.

Oxygen Channel—When Glu^{475}/Arg^{477}/Ile^{432} adopts the second conformation away from O-4 of the cofactor, a narrow channel extends from the bulk solvent to the substrate cavity and the isoalloxazine ring of the cofactor (Fig. 4*c*). This channel, positioned between β11 of the substrate-binding domain and the loop between α3 and β7 from the FAD-binding domain, is lined predominantly by hydrophobic side chains and is filled with a chain of 7 water molecules connected to each other through hydrogen bonds. In contrast, when Glu^{475}/Arg^{477}/Ile^{432} adopt the first conformation the water filled channel is sealed off from the substrate cavity and the cofactor (Fig. 4*d*).

Both the location and the hydrophobic nature of this channel suggest that it may serve as an entrance for molecular oxygen to the active site during the oxidative half-reaction. A hydrophobic channel has also been observed in the structures of cytochrome *c* oxidase (23–25) and the role of this channel as the oxygen pathway into the heme-copper site for O-2 reduction has been further supported by mutagenesis and kinetic studies (26). However, in flavoenzyme oxidases, where molecular oxygen is used to reoxidize the reduced flavin, such an oxygen channel has not previously been observed. In the structure of BCO2, control of oxygen access would be modulated by the position of Arg^{477} which acts as a "gate" adopting an open

conformation (Fig. 4, *a* and *c*) or a closed conformation (Fig. 4, *b* and *d*). Thus the side chain of Arg^{477} appears to control the entrance of oxygen to the active site in order for the oxidative half-reaction to proceed. The structure further suggests that the position of the gate may be controlled by the presence or absence of the steroid substrate.

It has recently been noted that the reaction of reduced BCO2 with dioxygen exhibits a peculiar behavior different from that of other flavoprotein oxidases (8). Specifically, the reaction of free, reduced BCO2 with molecular oxygen is biphasic; the first phase is fast and sensitive to oxygen concentration and the second phase is slower and insensitive to oxygen concentration. This behavior was proposed to reflect a reversible conversion of two species having substantially different oxygen reactivity. The alternate positions of the side chain of Arg^{477} and the role of this residue in gating oxygen access provides a rationale for the observed kinetic behavior. The fast phase may reflect the reaction of oxygen with the reduced cofactor through the channel in the "gate open" conformation. The slow phase would then correspond to the case in which oxygen access to the reduced flavin and reaction has to await a rate-limiting conformational change resulting in the opening of the gate. Clearly further mutagenesis and kinetic analysis would need to be carried out in order to confirm the role of Arg^{477} in controlling access of oxygen to the reduced flavin.

Steroid Bound Model—Kinetic comparisons of the two forms of cholesterol oxidase (BCO1 and BCO2) reveal significant differences in cholesterol binding (8). The structural differences observed between these two enzyme forms can be correlated to these observed kinetic differences. In the structures of the BCO1 (27–29) the substrate-binding site consists of a cavity, situated on the *re* face of the isoalloxazine ring, that houses only the four-ring system of cholesterol. The terpene chain extending from C-17 of the steroid D ring is not accommodated in the buried pocket; rather it is presumed to interact with a series of hydrophobic loops at the surface of the molecule. The structure of BCO2 also contains a large cavity that houses the four-ring system of the steroid substrate (Fig. 3*a*). However, a further extension from this cavity is of the appropriate size and dimension to bind the terpene portion of the substrate (the volume of cholesterol is 327 $Å^3$ based on van der Waals surface). Moreover, the hydrophobic nature of this extension makes it ideal for van der Waals interactions with the terpene moiety.

A model of the cholesterol bound complex is shown in Fig. 3*c* and clearly reveals the terpene-binding site. The interactions between the terpene moiety and the residues lining the extension can be correlated with a 10-fold increase in binding affinity observed for cholesterol in the case of the covalent form of the enzyme as compared with the non-covalent form (8). Comparisons of binding affinities of other steroid substrates that do not have a hydrophobic extension at C-17 of the steroid nucleus reveal significantly lower K_m values than that observed for cholesterol. Interestingly these steroids bind to the non-covalent form of the enzyme with higher affinities than to the covalent enzyme.

Further analysis of the modeled cholesterol-bound complex reveals that the best fit occurs when the arginine is in the "gate closed" conformation. This places C-3 and the hydroxyl group of the steroid substrate near to N-5 and O-4, respectively, of the cofactor. Furthermore, the steroid hydroxyl group is within hydrogen bonding distance from the guanidinium side chain of Arg^{477}. In the dehydrogenation reaction, a hydride is transferred from C-3 of the steroid substrate to N-5 of the cofactor resulting in the anionic form of reduced flavin, $FADH^-$. The gate closed conformation places the arginine side chain in a position where it can stabilize the negative charge on the pyrimidine moiety of the cofactor. In addition, concomitant with hydride transfer, a proton is abstracted from the C3-OH of the steroid. In the gate closed conformation, the carboxylate side chain of Glu^{475} lies 3.3 Å from the modeled steroid C3-OH suggesting it may function as the base for proton abstraction. Since Glu^{475} is also the proposed base for the isomerization step (see below), the proton abstracted during oxidation must be shuttled to another active site residue. The likely candidate for this proton shuttle would be Glu^{311}, which lies 2.6 Å from Glu^{475} (Fig. 4*a*) and is held in position by interactions with Tyr^{422} and Lys^{324}. Furthermore, Glu^{311} lies near to the gated entrance for molecular oxygen. In the gate open conformation, the carboxylate of Glu^{311} hydrogen bonds to the guanidinium side chain of Arg^{477} (Fig. 4*b*) suggesting that, upon opening of the gate, the Arg^{477}-Glu^{311} interaction may facilitate proton transfer to the incoming oxygen molecule during the oxidative half-reaction.

In addition to oxidation, cholesterol oxidase also carries out an isomerization reaction, shifting the double bond from Δ^5 to Δ^4 of the steroid intermediate. In BCO1 structural (6, 29) and mutagenesis and kinetic studies (30) have indicated that a single glutamate residue (Glu^{361}) functions as the acid/base in proton abstraction from C-4 and reprotonation at C-6 of the steroid. The steroid bound model for BCO2 also reveals a glutamate (Glu^{475}) near to the isomerization center. The position of Glu^{475} and the alternate conformations observed suggest that it may function in an identical fashion to Glu^{361} in BCO1. In the gate closed conformation, the carboxylate moiety of Glu^{475} lies near to C-4 of the steroid A ring, well positioned for proton abstraction. Upon rearrangement of the Arg-Glu pair to the gate open conformation the glutamate carboxylate moves closer to C-6 where reprotonation would occur. In addition, the gate open conformation of Glu^{475} results in an unfavorable interaction with the C-19 methyl group of the steroid, thus destabilizing the binding of the steroid and promoting product release. Finally, the release of the product and the opening of the gate would enable the binding of oxygen in proximity to C4a of the cofactor where reduction to peroxide is known to occur. Such a sequence of events is consistent with the observed ping-pong mechanism for BCO2 (8).

In conclusion, the structure of BCO2 adopts a different fold from that seen for BCO1. These differences reveal a number of novel features that can be correlated with observed differences in kinetic features between the two enzyme forms. In particular, the structure of BCO2 reveals a substrate-binding site that is able to house an entire cholesterol molecule including the terpene moiety. Furthermore, this structure supports kinetic data used to propose a mechanism for BCO2 catalysis and identifies specific residues important for each of the catalytic events. The structure provides us with a unique view of how molecular oxygen may access the active site of a flavoenzyme and how side chain mobility may control this access during the oxidative half-reaction.

Acknowledgments—We thank Roche Diagnostics for the generous supply of BCO2. We also thank B. Ahvazi for technical assistance and P. Pawelek and P. Lario for helpful discussion.

REFERENCES

1. Corbin, D. R., Greenplate, J. T., Wong, E. Y., and Purcell, J. P. (1994) *Appl. Environ. Microbiol.* **60,** 4239–4244
2. Greenplate, J. T., Duck, N. B., Pershing, J. C., and Purcell, J. P. (1995) *Entomol. Exp. Appl.* **74,** 253–258
3. Purcell, J. P., Greenplate, J. T., Jennings, M. G., Ryerse, J. S., Pershing, J. C., Sims, S. R., Prinsen, M. J., Corbin, D. R., Tran, M., Sammons, R. D., and Stonard, R. J. (1993) *Biochem. Biophys. Res. Commun.* **196,** 1406–1413
4. Corbin, D. R., Greenplate, J. T., and Purcell, J. P. (1998) *Hortscience* **33,** 614–617
5. Ghoshroy, K. B., Zhu, W., and Sampson, N. S. (1997) *Biochemistry* **36,** 6133–6140

6. Li, J., Vrielink, A., Brick, P., and Blow, D. M. (1993) *Biochemistry* **32,** 11507–11515
7. Sampson, N. S., Kass, I. J., and Ghoshroy, K. B. (1998) *Biochemistry* **37,** 5770–5778
8. Pollegioni, L., Wels, G., Pilone, M. S., and Ghisla, S. (1999) *Eur. J. Biochem.* **263,** 1–13
9. Croteau, N., and Vrielink, A. (1996) *J. Struct. Biol.* **116,** 317–319
10. Otwinowski, Z., and Minor, W. (1997) in *Methods in Enzymology* (Carter, C. W., Jr., and Sweet, R. M., eds) pp. 307–326, Academic Press, London
11. Otwinowski, Z. (1993) in *Data collection and Processing: Proceedings of the CCP4 Study Weekend* (Sawyer, L., Isaccs, N., and Bailey, S., eds) pp. 56–62, SERC Daresbury Laboratory, Warrington, United Kingdom
12. Abrahams, J. P., and Leslie, A. G. W. (1996) *Acta Crystallogr. Sect. D* **52,** 30–42
13. Jones, T. A., Zou, J.-Y., Cowan, S. W., and Kjeldgaard, M. (1991) *Acta Crystallogr. Sect. A* **47,** 110–119
14. Brünger, A. T., Adams, P. D., Clore, G. M., DeLano, W. L., Gros, P., Grosse-Kunstleve, R. W., Jiang, J.-S., Kuszewski, J., Nilges, M., Pannu, N. S., Read, R. J., Rice, L. M., Simonson, T., and Warrem, G. L. (1998) *Acta Crystallogr. Sect. D* **54,** 905–921
15. Laskowski, R. A., MacArthur, M. W., Moss, D. S., and Thornton, J. M. (1993) *J. App. Crystallogr.* **26,** 283–291
16. Berman, H. M., Westbrook, J., Feng, Z., Gilliland, G., Bhat, T. N., Weissig, H., Shindyalov, I. N., and Bourne, P. E. (2000) *Nucleic Acids Res.* **28,** 235–242
17. Mattevi, A., Fraaije, M. W., Mozzarelli, A., Olivi, L., Coda, A., and van Berkel, W. J. H. (1997) *Structure* **5,** 907–920
18. Benson, T. E., Filman, D. J., Walsh, C. T., and Hogle, J. M. (1995) *Nat. Struct. Biol.* **2,** 644–653
19. Dobbek, H., Gremer, L., Meyer, O., and Huber, R. (1999) *Proc. Natl. Acad. Sci. U. S. A.* **96,** 8884–8889
20. Mathews, F. S., Chen, Z.-W., and Bellamy, H. D. (1991) *Biochemistry* **30,** 238–247
21. Fraaije, M. W., van Berkel, W. J. H., Benen, J. A. E., Visser, J., and Mattevi, A. (1998) *Trends Biochem. Sci.* **23,** 206–207
22. Mewies, M., McIntire, W. S., and Scrutton, N. S. (1998) *Protein Sci.* **7,** 7–20
23. Iwata, S., Ostermeier, C., Ludwig, B., and Michel, H. (1995) *Nature* **376,** 660–669
24. Riistama, S., Puustinen, A., Garciahorsman, A., Iwata, S., Michel, H., and Wikstrom, M. (1996) *Biochim. Biophys. Acta Bioenerg.* **1275,** 1–4
25. Soulimane, T., Buse, G., Bourenkov, G. P., Bartunik, H. D., Huber, R., and Than, M. E. (2000) *EMBO J.* **19,** 1766–1776
26. Riistama, S., Puustinen, A., Verkhovsky, M. I., Morgan, J. E., and Wikstrom, M. (2000) *Biochemistry* **39,** 6365–6372
27. Vrielink, A., Lloyd, L. F., and Blow, D. M. (1991) *J. Mol. Biol.* **219,** 533–554
28. Vrielink, A., Li, J., Brick, P., and Blow, D. M. (1994) in *Flavins and Flavoproteins* (Curti, B., Ronchi, S., and Zanetti, G., eds) pp. 175–184, Water de Gruyter & Co., Berlin
29. Yue, Q. K., Kass, I. J., Sampson, N. S., and Vrielink, A. (1999) *Biochemistry* **38,** 4277–4286
30. Kass, I. J., and Sampson, N. S. (1998) *Bioorg. Medi. Chem. Lett.* **8,** 2663–2668
31. Kraulis, P. (1991) *J. Appl. Crystallogr.* **24,** 946–950
32. Nicholls, A., Sharp, K., and Honig, B. (1991) *Proteins* **11,** 281–296